Schweizerischer Erdbebendienst
Service Sismologique Suisse
Servizio Sismico Svizzero
Swiss Seismological Service

ETH zürich

SITE CHARACTERIZATION REPORT

SSTS: Stans (NW) - Spital

Agostiny Marrios Lontsi, Clotaire Michel, Manuel Hobiger, Donat Fäh

Last Modification: 28th May, 2020

Schweizerischer Erdbebendienst (SED)
Service Sismologique Suisse
Servizio Sismico Svizzero
Servizi da Terratrembels Svizzer

ETH Zürich
Sonneggstrasse 5
8092 Zürich
Schweiz
agostiny.lontsi@sed.ethz.ch

Contents

Summary

A passive seismic survey was conducted at the strong-motion site SSTS at Stans, Canton of Nidwalden, Central Switzerland, to characterize the underlying subsurface. The site characterization aims at inferring the shear-wave velocity profile. The passive seismic array consisted of 16 3C Le3D/5sec seismic sensors with a 2D spiral-arm configuration. The minimum and maximum interstation distances were 7.9 and 446.39 m, respectively. Surface wave methods were used to extract the Rayleigh wave ellipticity from single station recordings and the phase velocity dispersion curves of both Rayleigh and Love waves. The ellipticity is extracted in the frequency range from 0.2 to 50 Hz. We observe two major peak amplitudes at about 0.7 and 8 Hz.

The used array methods, that include the frequency-wavenumber, the wavefield decomposition, and the spatial autocorrelation, provide clear phase velocity dispersion curves for the Rayleigh and Love waves. Two Rayleigh wave branches are observed and interpreted as fundamental and first higher modes. One Love wave branch is observed and interpreted as fundamental mode.

The combined inversion considers (1) the ellipticity peak frequency at 0.7 Hz, (2) the left and right flank of the ellipticity peak at 8 Hz, (3) the fundamental and first higher mode of the Rayleigh, and (4) the fundamental mode of the Love waves phase velocity dispersion curves. Different parametrizations that consider 3, 4, 5, 6, 7, and 24 (with fixed layer thicknesses) layers over halfspace were used. The resulting best velocity profiles indicate three major discontinuities at around 3.5, 12, and 300 m depth. We consider each of these best models to be representative of the underground structure at the strong motion station. The average V_{S30} from the best shear wave velocity profiles of the site is 385.25 $\pm$ 9.43 m/s. This V_{S30} value corresponds to ground type B in EC8 (European standard) and to ground type C in SIA261 (Swiss standard).

1 Introduction

As part of the Swiss Strong Motion Network renewal project phase 2, a strong motion station was built close to the cantonal hospital of Nidwalden in Stans. The station went operational on March 13th, 2015. At this site, a passive seismic survey was performed to record the propagating ambient noise wavefield. We use surface wave methods to analyze the contribution of Rayleigh and Love waves to the recorded noise wavefields. The estimated phase velocity dispersion and the ellipticity information are combined in an inversion process to infer the underlying subsurface structure and the corresponding 1D shear wave velocity profile.

2 Site and geological setting

Stans is the capital of the canton of Nidwalden, located in central Switzerland. The near subsurface geology consists of quaternary alluvia, creek deposits, and moraine (Figure 1). The northern stations of the array deployment were located on alluvial deposits, the southern ones on creek deposits.

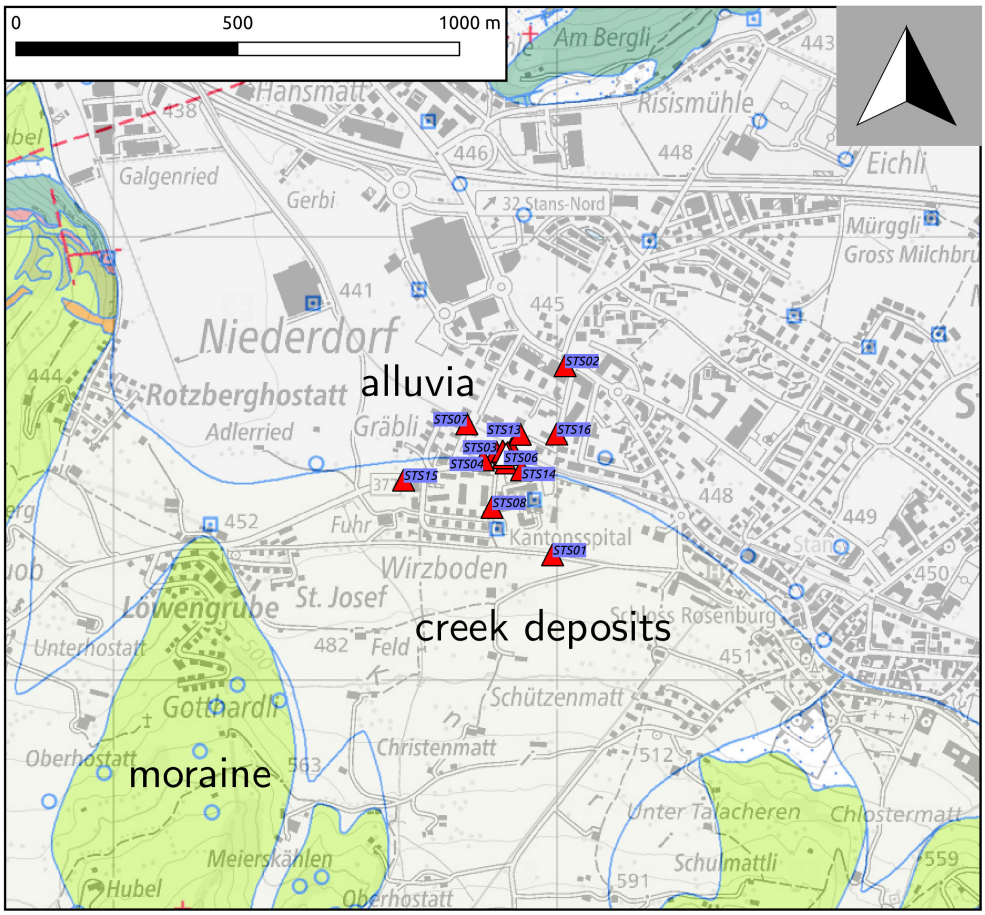

Figure 1: Site and geological setting. ©2019 swisstopo (JD100042)

3 Overview of the site characterization measurement

Figure 2 shows an aerial image of the survey site, indicating the permanent station SSTS and the stations STS01-STS16 of the passive array measurements.

Figure 2: Background topography, strong motion station location and array configuration

In order to characterize the local underground structure around station SSTS, a passive seismic array measurements was carried out on September 29^{th}, 2017. The layout of the seismic measurements is shown in Figure 2. The array consisted of 16 stations. It was planned to consist of five rings of three stations each around a central station. The minimum and maximum inter-station distances of the final array layout were 7.9 and 446.39 m, respectively. The names of the stations of the first array are composed of "STS" followed by a two-digit number (01 to 16). The seismic stations consisted of Lennartz 3C 5 s sensors connected to Centaur digitizers. A total of 12 digitizers were used. Twelve sensors were connected to the A channels of the digitizers and another four sensors were connected to the B channels.
The data of the complete array were analyzed together and also as sub-array excluding the outermost stations (STS01, STS02, STS08, and STS15), resulting in a smaller array with more homogeneous underground. The maximum inter-station distance for the small array was 200 m. The array continously recorded ambient vibrations for 3h5min. The station locations have been measured by a differential GPS system (Leica Viva GS10) which was set up to measure with a precision better than 5 cm. This precision was achieved for all stations.

4 Single station analysis

4.1 Microtremor H/V and ellipticity estimation

The microtremor H/V spectral ratio and the ellipticity are obtained using 6 different techniques:

- geopsyhv: full microtremor H/V estimation (www.geopsy.org; Last accessed: January 7^{th}, 2020);
- RayDec, optimized for Rayleigh wave ellipticity estimation (Hobiger et al., 2009);
- FTAN, optimized for Rayleigh wave ellipticity estimation (**?**);
- CLASS, optimized for Rayleigh wave ellipticity estimation, (Fäh et al., 2001);
- VPTFA, optimized for Rayleigh wave ellipticity estimation (Poggi & Fäh, 2010);
- MTSPEC, optimized for Rayleigh wave ellipticity estimation (**?**).

The H/V results for each station using the 6 techniques are shown in Figure 3 for comparison. In general, the H/V spectral ratio shows two to three peak frequencies. For each station, two peak frequencies are picked between 0.2 and 20 Hz (Figure 4).

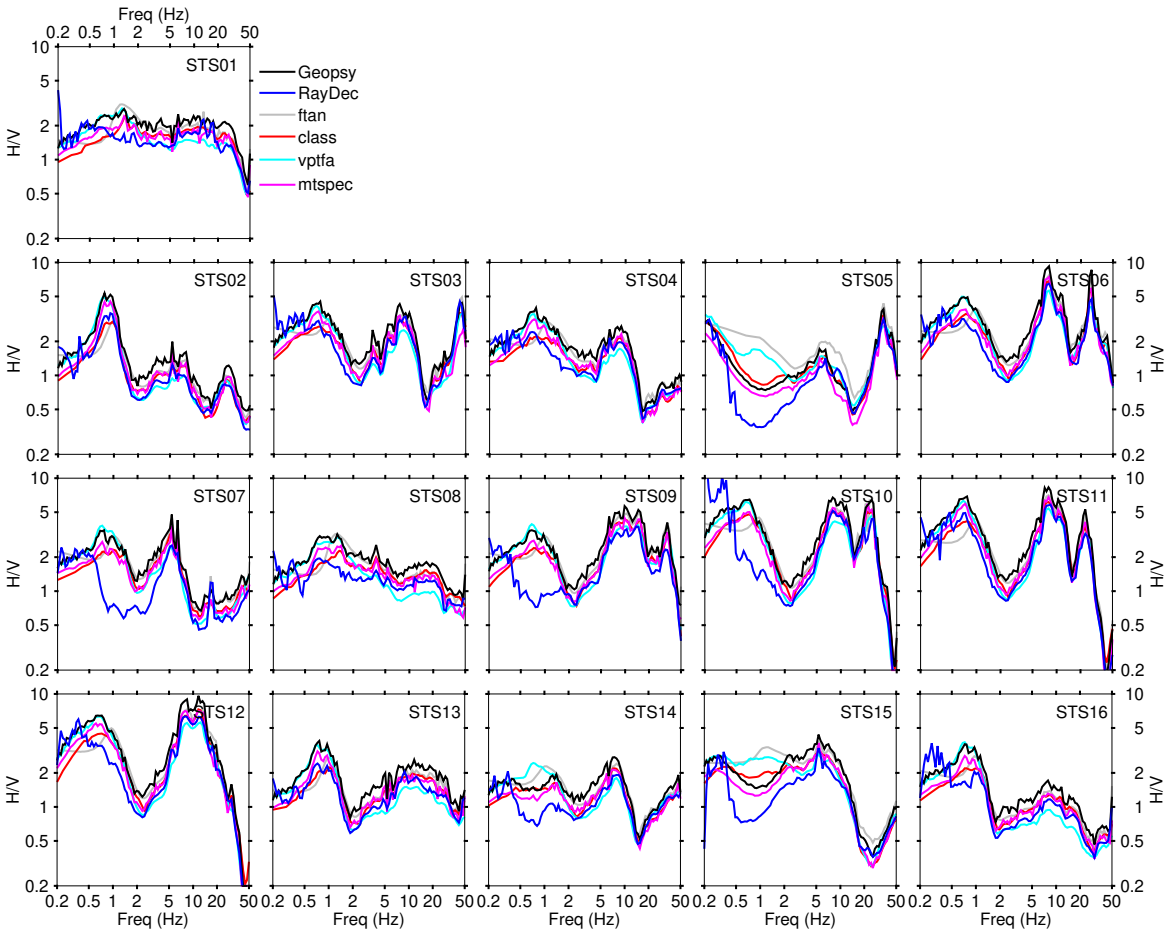

Figure 3: H/V spectral ratio estimation estimation using different techniques.

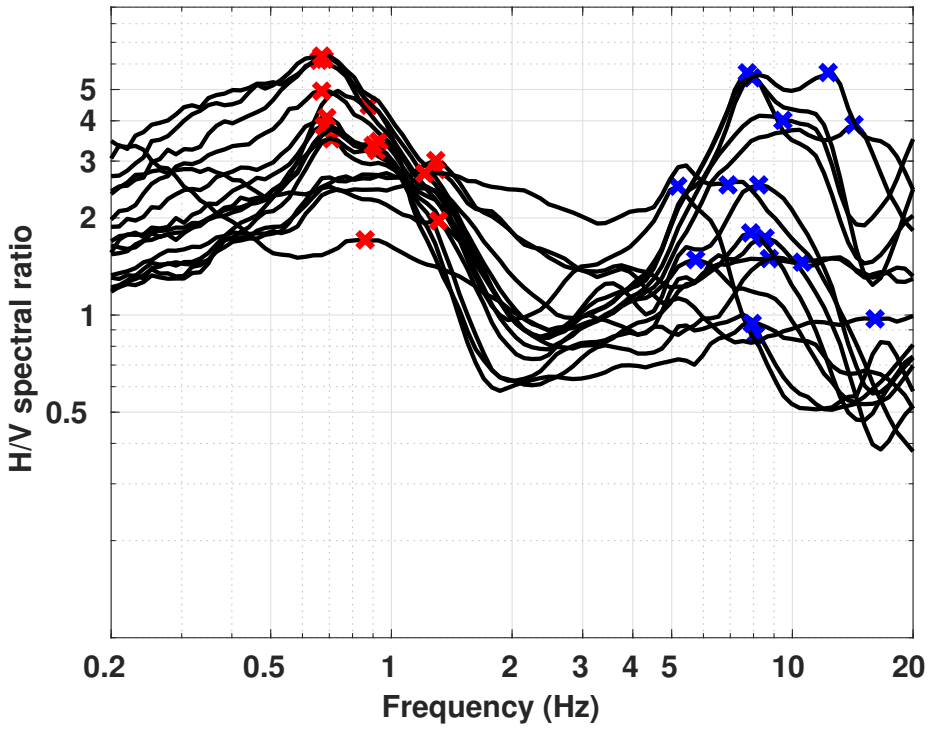

Figure 4: Overview of the H/V curves of the different stations, obtained using the ellipticity technique by **?**.

The first peak frequency for all stations varies from 0.66 to 1.31 Hz and the second peak frequency from 5.18 to 16.08 Hz. The presence of more than one frequency peak suggests that the subsurface structure has more than one strong impedance contrast. The depth of the impedance contrast is highly variable. The variation in the H/V amplitude around the peak frequency indicates also high variability in the impedance contrast.

4.2 Polarization analysis

Following **??**, the polarization analysis is performed to assess potential 2D effects. The results are shown in Figure 5 for station STS11, the central station of the array.

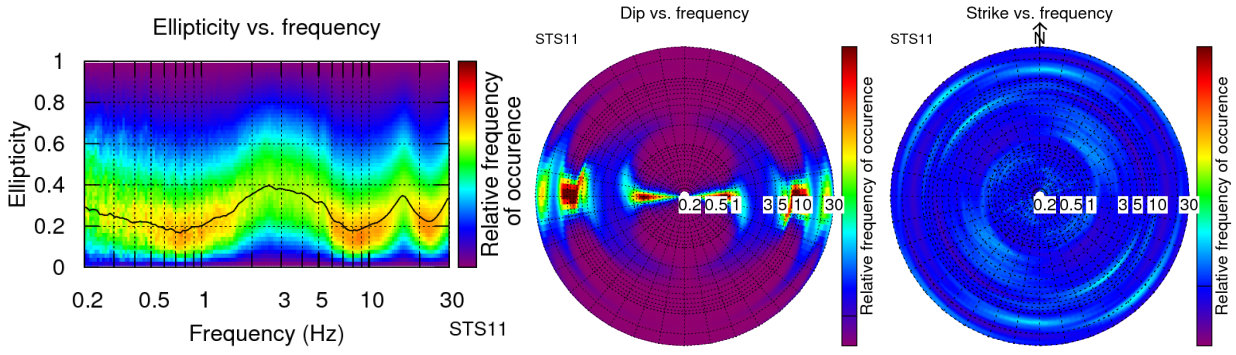

Figure 5: Polarization analysis for the station STS11 located next to the permanent station.

We cannot see a preferential strike direction and no indications for 2-dimensional polarization effects.

5 Array analysis

The phase velocities for Rayleigh and Love waves are estimated both using the full array of 16 stations and the small array of 12 stations, using three different array methods:

- High resolution frequency-wavenumber (HRFK, Poggi & Fäh 2010);
- Wavefield decomposition (WaveDec, Maranò et al. 2012);
- Spatial autocorrelation (SPAC, Aki 1957; Bettig et al. 2001).

The results of the dispersion curve analysis are presented in Figures 6-7 for the HRFK, in Figure 8 for the WaveDec, and in Figure 9 for the SPAC.

5.1 HRFK

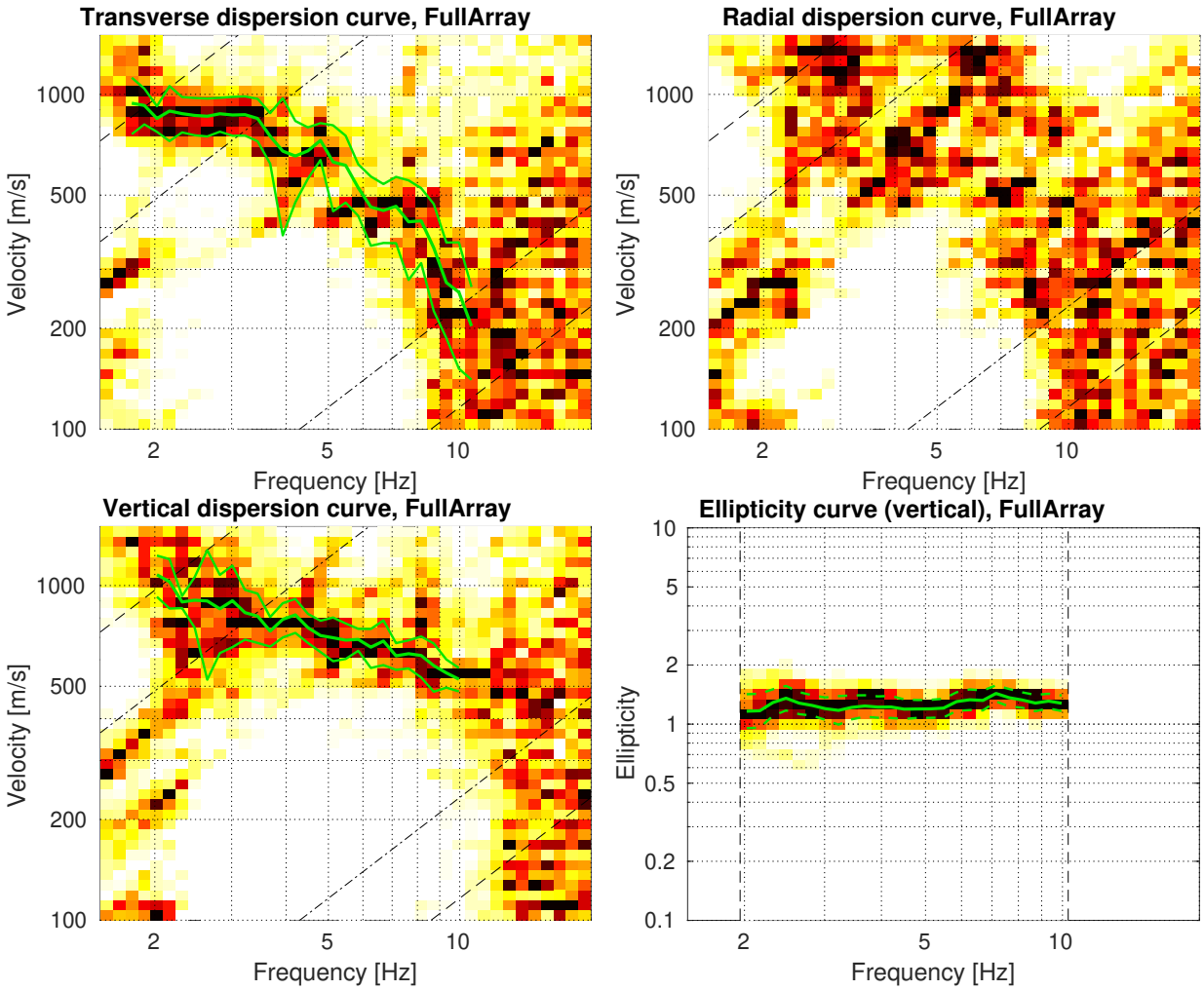

Figure 6: HRFK results with 16 stations (FullArray). The phase velocity dispersion curves on the three components together with the ellipticity are shown. The phase velocity dispersion branches are picked within the array resolution limits on the transverse component for Love waves and on the vertical for Rayleigh waves. The dashed and dotted black lines are the array resolution limits. The solid green curves are picked from the data, where the central line indicates the best values and the two outer curves the standard deviation.

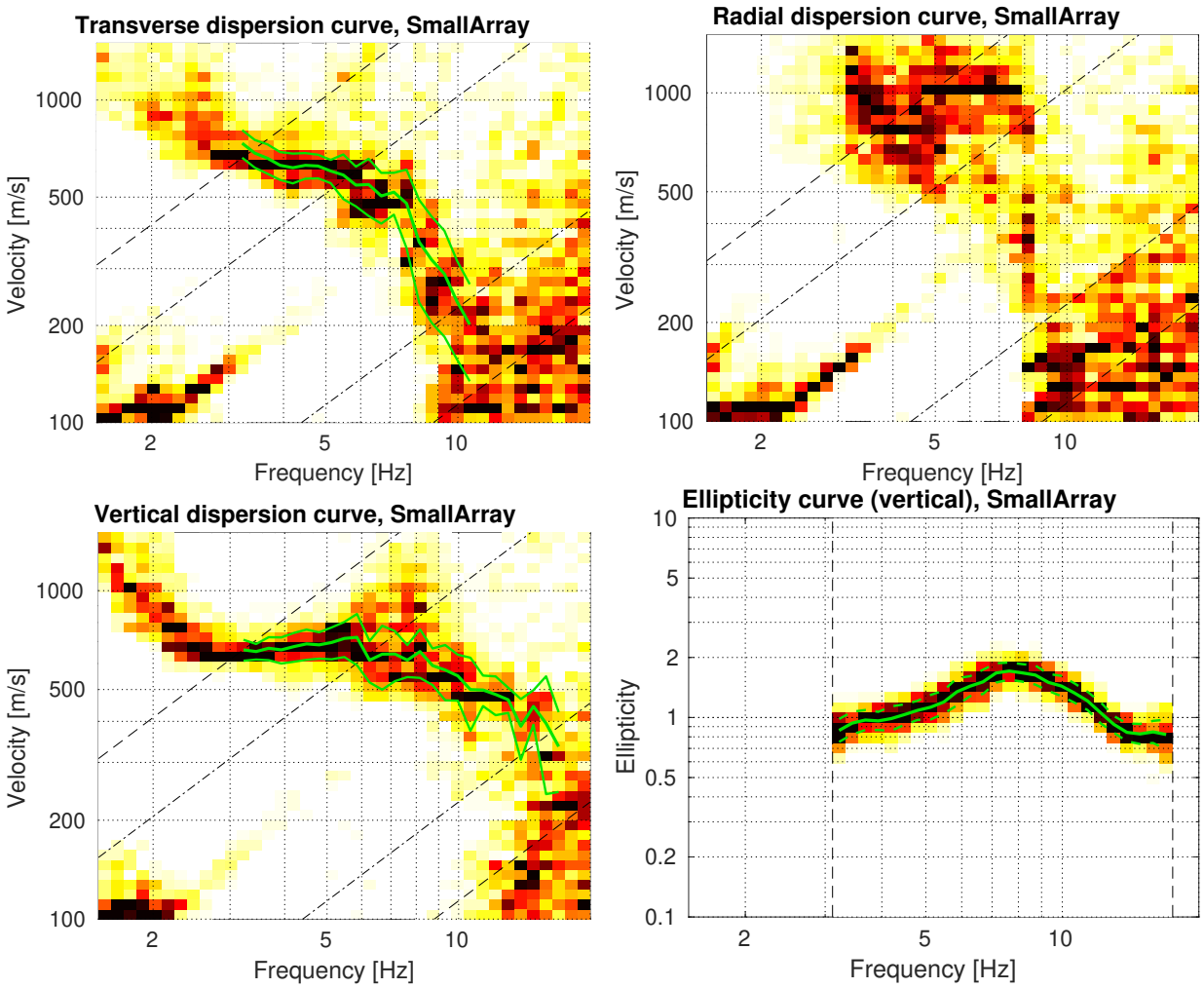

Figure 7: HRFK results with 12 stations (SmallArray). The phase velocity dispersion curves on the three components together with the ellipticity are shown. The phase velocity dispersion branches are picked within the array resolution limits on the transverse component for Love waves and on the vertical for Rayleigh waves. The dashed and dotted black lines are the array resolution limits. The solid green curves are picked from the data, where the central line indicates the best values and the two outer curves the standard deviation.

For both the large and the small array, we picked within the resolution limits (represented by the dashed and dotted black lines in Figures 6 and 7) the transverse (Love waves) and vertical (Rayleigh waves) phase velocity dispersion curves (represented by the green curves).
The integration of the results from the large and small array allow us to obtain phase velocity dispersion curves for Rayleigh and Love waves in a very large frequency band that ranges from 1.77 to 16.94 Hz.

5.2 WaveDec

Clear phase velocity dispersion curves are also observed for both Rayleigh and Love waves in the frequency range from 2.75 to 12.76 Hz. The ellipticity curve was picked in the frequency range of the Rayleigh wave dispersion curve. Over the whole frequency range, the particle motion is retrograde.

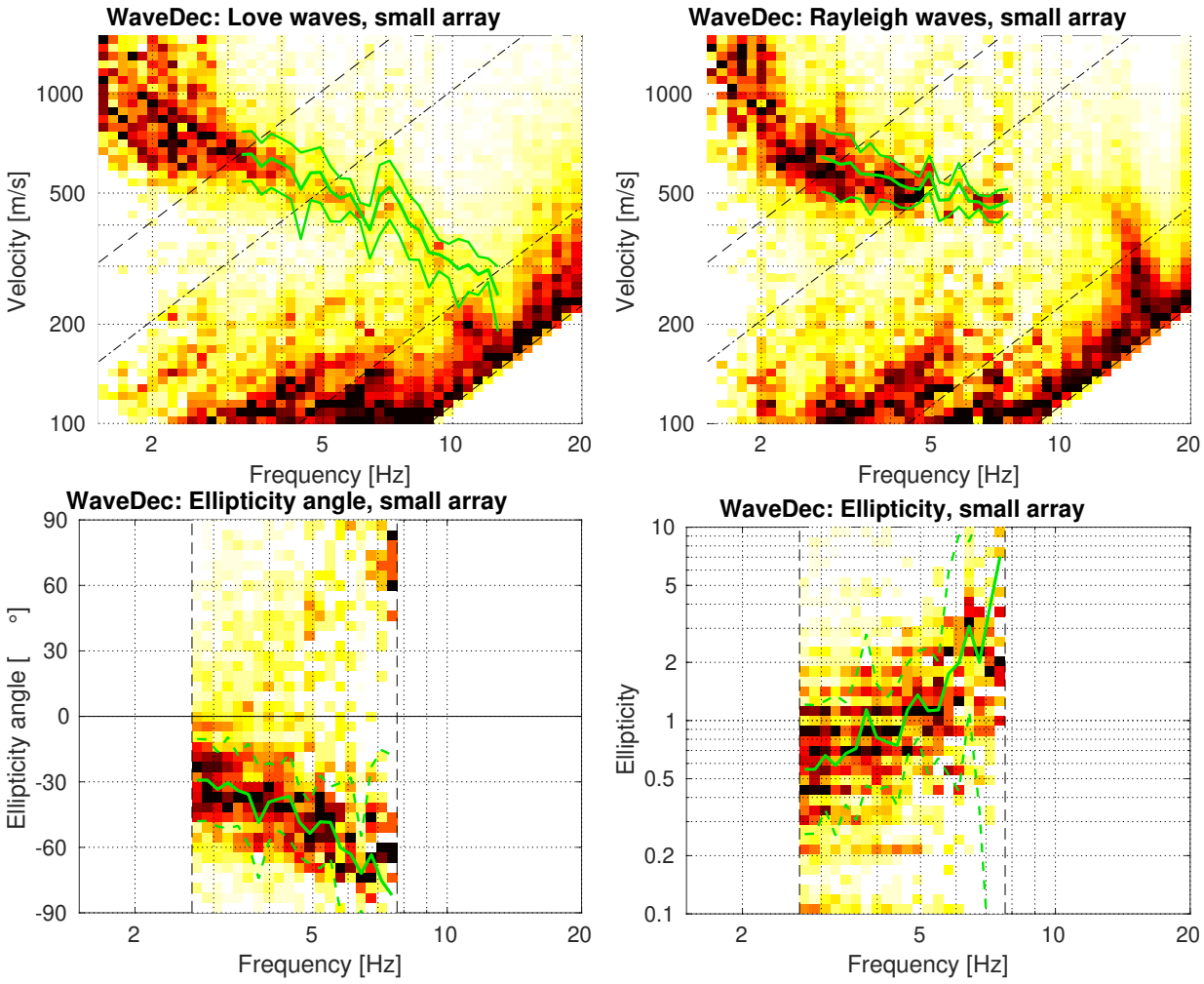

Figure 8: WaveDec with 12 stations: ellipticity and velocity dispersion curves for Rayleigh and Love waves. The phase velocity dispersion branches are picked within the array resolution limits. The solid green curves are picked from the data, where the central line indicates the best values and the two outer curves the standard deviation.

5.3 SPAC

The SPAC (Aki, 1957) curves of the vertical components have been calculated using the M-SPAC (Bettig et al., 2001) technique implemented in geopsy. Rings with different radius ranges had been defined and for all station pairs with distance inside this radius range, the cross-correlation was calculated over a wide frequency range. These cross-correlation curves are averaged for all station pairs of the respective ring and give the SPAC curves.

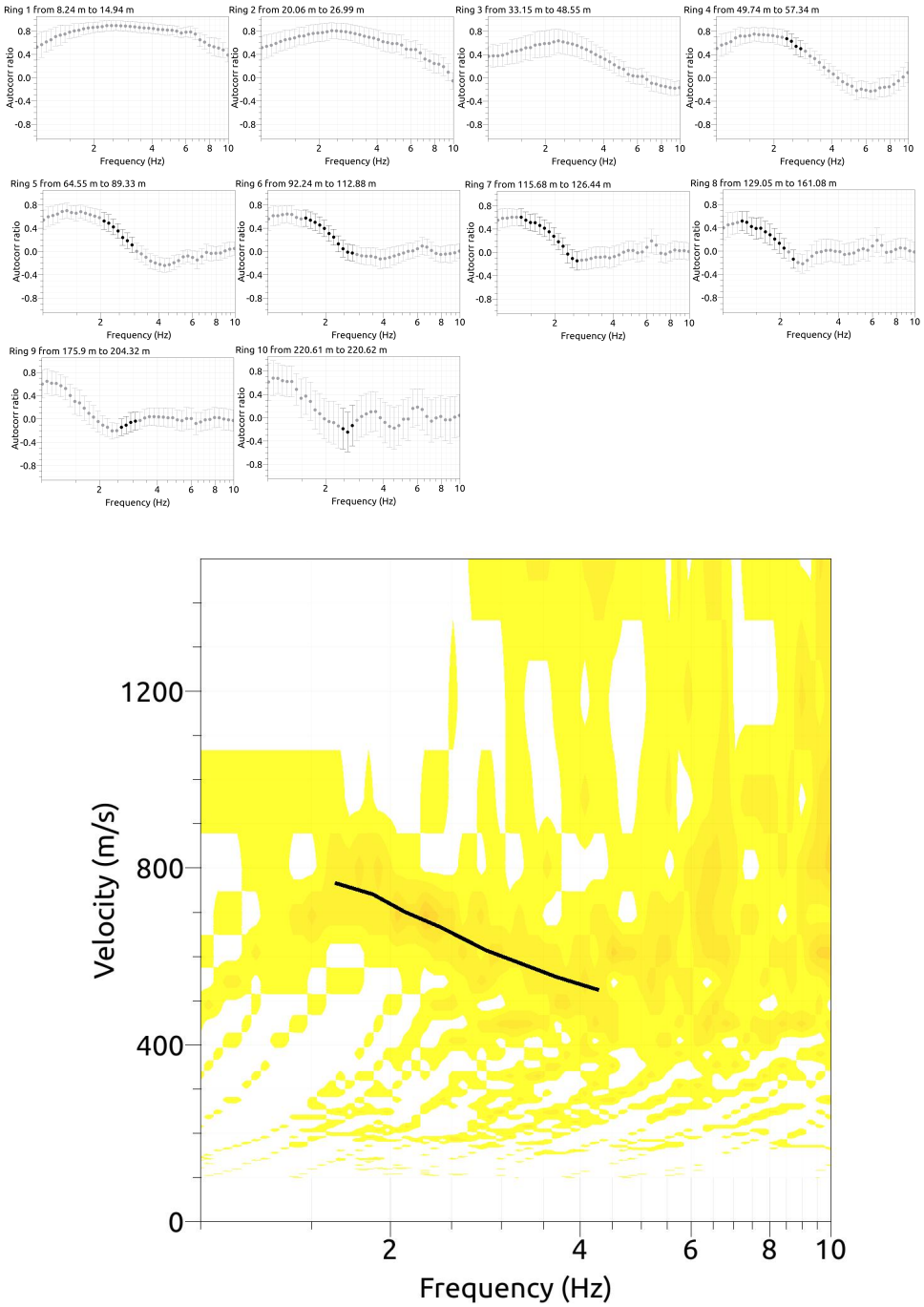

Figure 9: SPAC with 12 stations. The picked phase velocity dispersion branch is represented by the black curve.

The SPAC curves for all defined rings are shown in Figure 9. The phase velocity is obtained through a non-linear inversion of the autocorrelation coefficients. This was made with the function spac2disp of the geopsy package. Using SPAC, we can retrieve a Rayleigh wave dispersion curve between 1.66 and 4.2 Hz.
The phase velocity dispersion curves from SPAC contains information below 2 Hz. Information below this frequency is not observed with the HRFK and WaveDec techniques.

5.4 Overview and discussion of the measurement results

A summary of the estimated dispersion curve branches using the HRFK, WaveDec, and SPAC methods is presented in Figure 10. Two distincts branches are observed for the Rayleigh waves. The first branch is obtained by combining results from WaveDec and SPAC. SPAC gives a dispersion curve at lower frequencies than the other methods, down to 1.66 Hz. The second branch is obtained by integrating HRFK results of the full and small array processings. The Love wave dispersion curves for the different methods are in good agreement.
It is not clear whether the dispersion curve from HRFK FullArray (red dots) below 3.28 Hz for the Love waves represents a higher mode or not. The Rayleigh wave branch dispersion curve from HRFK (red dots) poses the same challenge below 5 Hz. For the next steps, we try to interpret the first branch between 1.66 Hz and 7.51 Hz and the second branch between 6.97 and 15.95 Hz. The Love wave branch is interpreted between 3.28 and 10.15 Hz.
Assigning a mode number to the velocity dispersion branches is an important step towards a reliable combined inversion. To interpret the different branches of the velocity dispersion curves, a blind mode search was performed. One branch was assigned the fundamental mode and additional branches were allowed to correspond to any higher mode. It comes out that the Rayleigh wave dispersion curve branches correspond to the fundamental and first higher modes (10b and 10c), respectively, and the Love wave branch corresponds to the fundamental mode (see Figure 10e). The attempt to include information beyond these frequency ranges did not improve our results.
The ellipticity curves estimated using RayDec, HRFK, and WaveDec are shown in Figure 10(f). The RayDec curve for station STS11, the central station of the array, shows a fundamental peak around 0.7 Hz and a second higher peak around 8 Hz. The curves from the other stations of the array were different (see Figure 3). The WaveDec ellipticity curve was estimated using the small array and is in good agreement with the RayDec curve. In the frequency range accessible to the array analysis, the particle motion of the Rayleigh waves was detected as retrograde by WaveDec, which is in agreement with the particle motion of the left flank of the second peak determined by RayDec. It is unclear if the two peaks are singularities or not. The HRFK ellipticity estimations using both arrays are different and differ from the other methods. Therefore, we will neglect these curves. For the combined inversion, the interpreted ellipticity and dispersion curves of Rayleigh and Love waves are used (Figure 10).

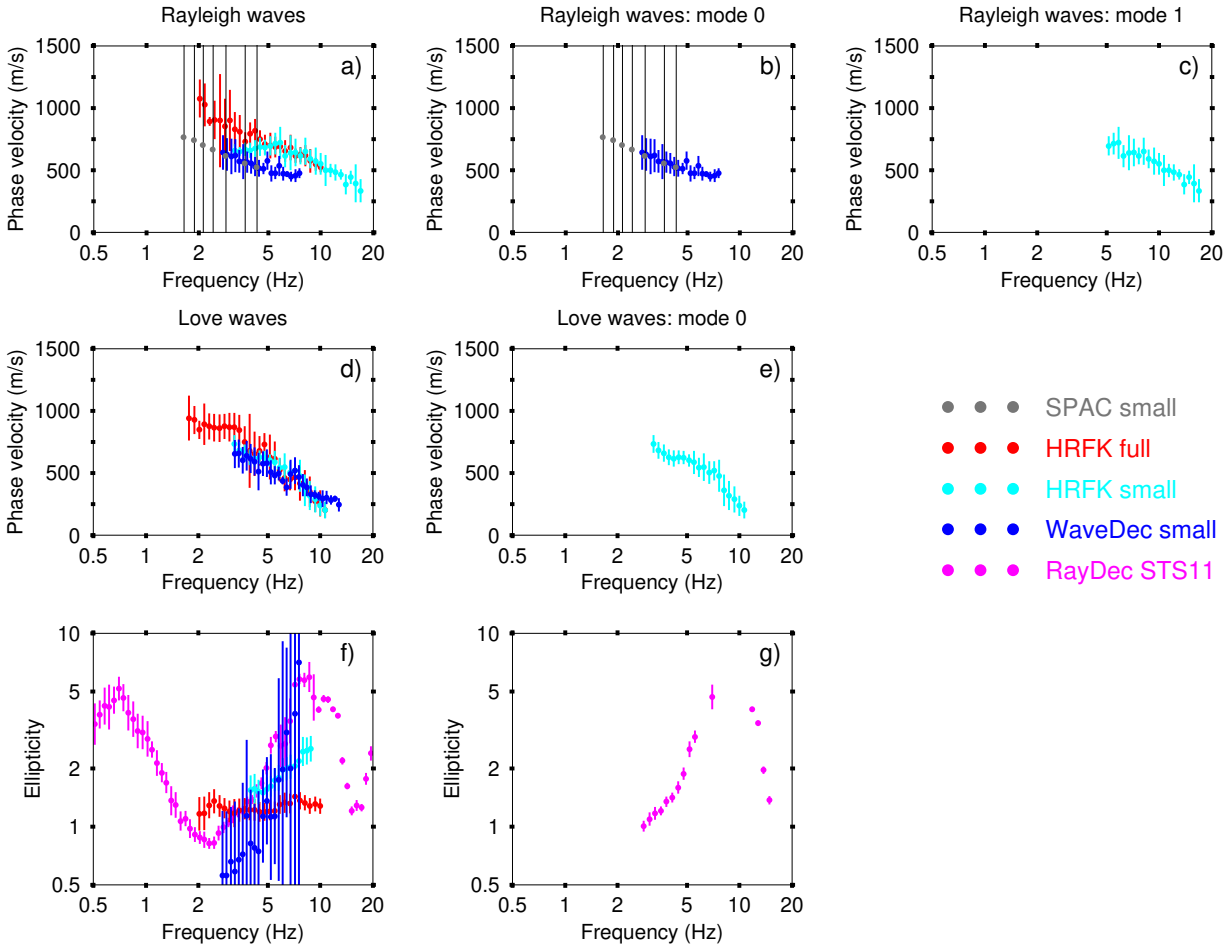

Figure 10: Overview of the results and interpreted curves obtained using the different analysis methods. a) Estimated Rayleigh wave dispersion curves. b) Interpreted Rayleigh wave phase velocity fundamental mode. c) Interpreted Rayleigh wave phase velocity first higher mode. d) Estimated Love wave dispersion curves. e) Interpreted Love wave phase velocity fundamental mode. f) Estimated Rayleigh wave ellipticity. g) Ellipticity around the peak frequency at 8 Hz. This information together with the peak frequency at 0.7 Hz are used with the dispersion curve information in the inversion.

6 Inversion

6.1 Parametrization

The inversion assumes a layered earth structure. Three, four, five, six and seven layers over half-space were used, as well as a parameter space with fixed layer depths. The inversion uses the global search neighborhood algorithm (Sambridge, 1999; Wathelet, 2008). The process is started with a set of 50 models. In each iteration step, 50 new models are generated and 50 best models are kept for further analysis. The process is iterated a large number of times, in this case 4000 times. This results in 200050 generated models. The choice of the parameters for the neighborhood algorithm ensures that we sufficiently explore and exploit the parameter space.

6.2 Results

Figures 11-16 show the inversion results. We summarise and interpret the best profiles from the inversion in Figure 17.

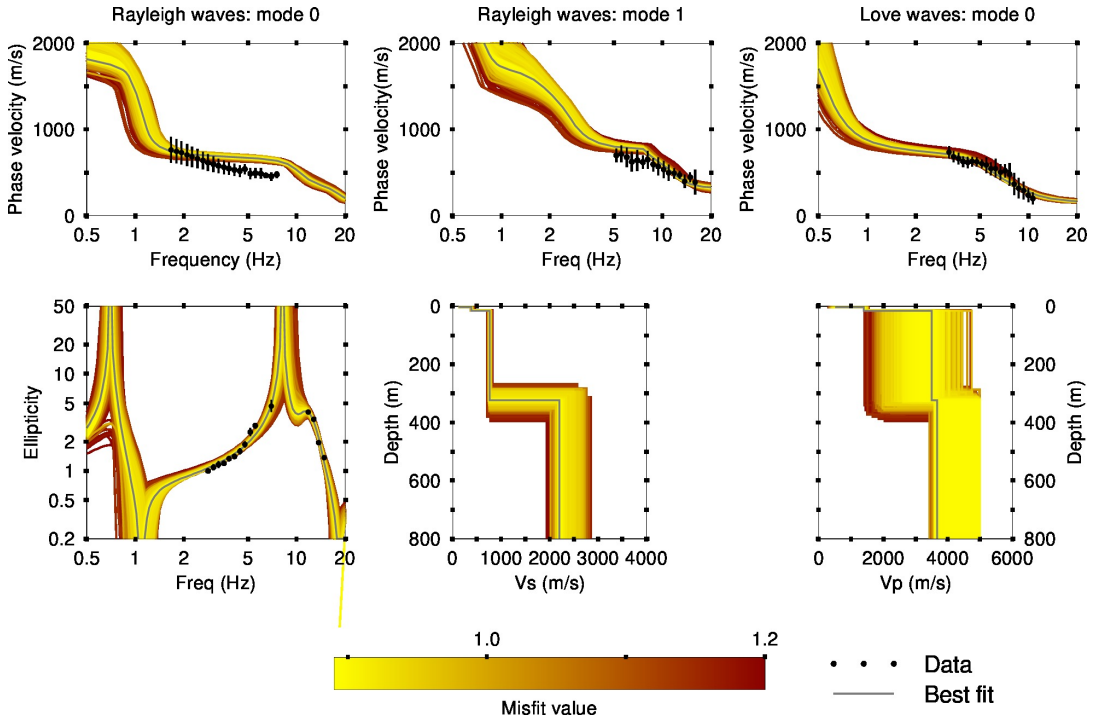

Figure 11: Inversion results using a 3LOH parametrization. The different models are shown in a color according to the misfit value, where the best model is shown in continuous grey color and the black dots indicate the data points that contribute to the inversion. The peak frequency at 0.7 Hz is used to constrain the bottom depth.

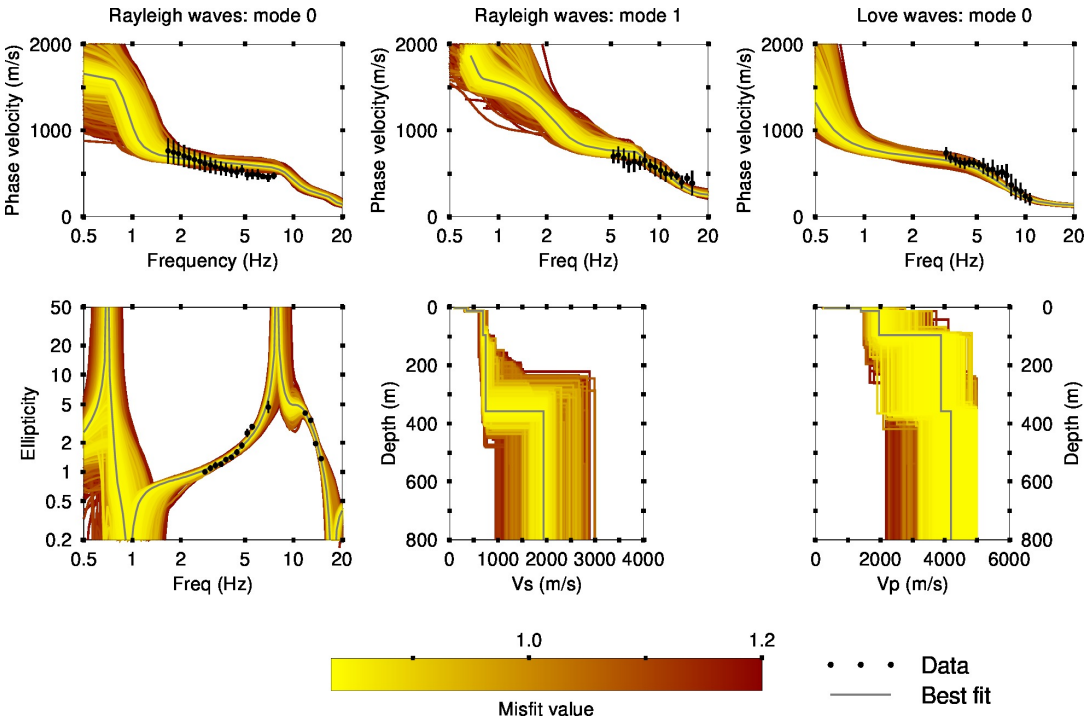

Figure 12: Inversion results using a 4LOH parametrization. The different models are shown in a color according to the misfit value, where the best model is shown in continuous grey color and the black dots indicate the data points that contribute to the inversion. The peak frequency at 0.7 Hz is used to constrain the bottom depth.

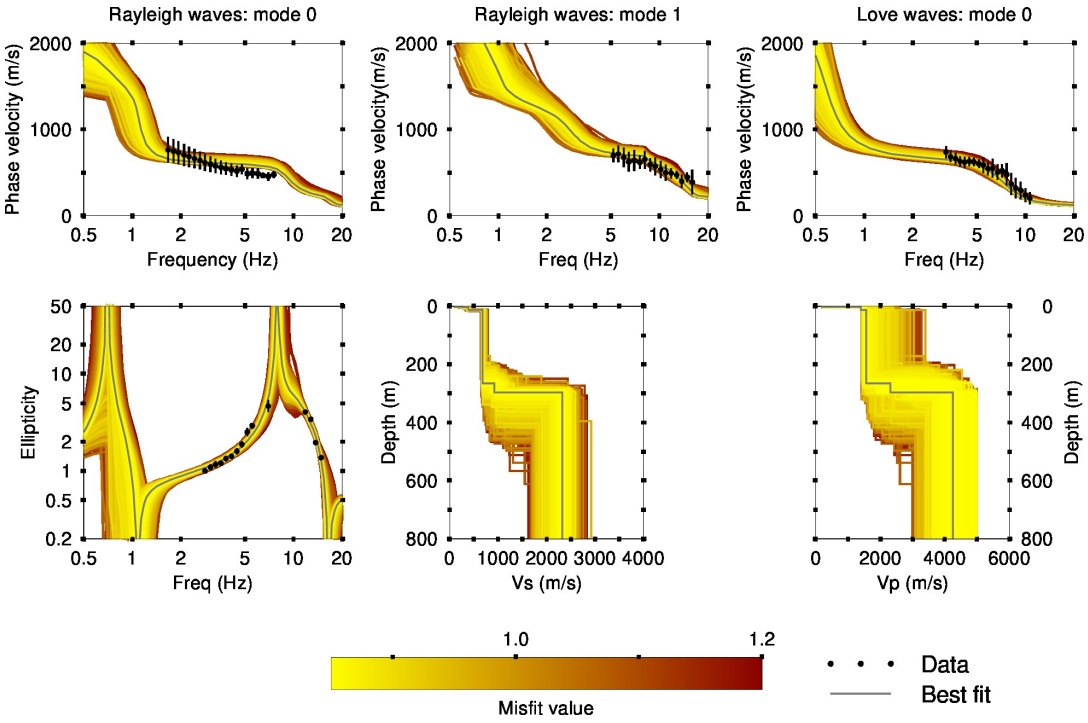

Figure 13: Inversion results using a 5LOH parametrization. The different models are shown in a color according to the misfit value, where the best model is shown in continuous grey color and the black dots indicate the data points that contribute to the inversion.The peak frequency at 0.7 Hz is used to constrain the bottom depth.

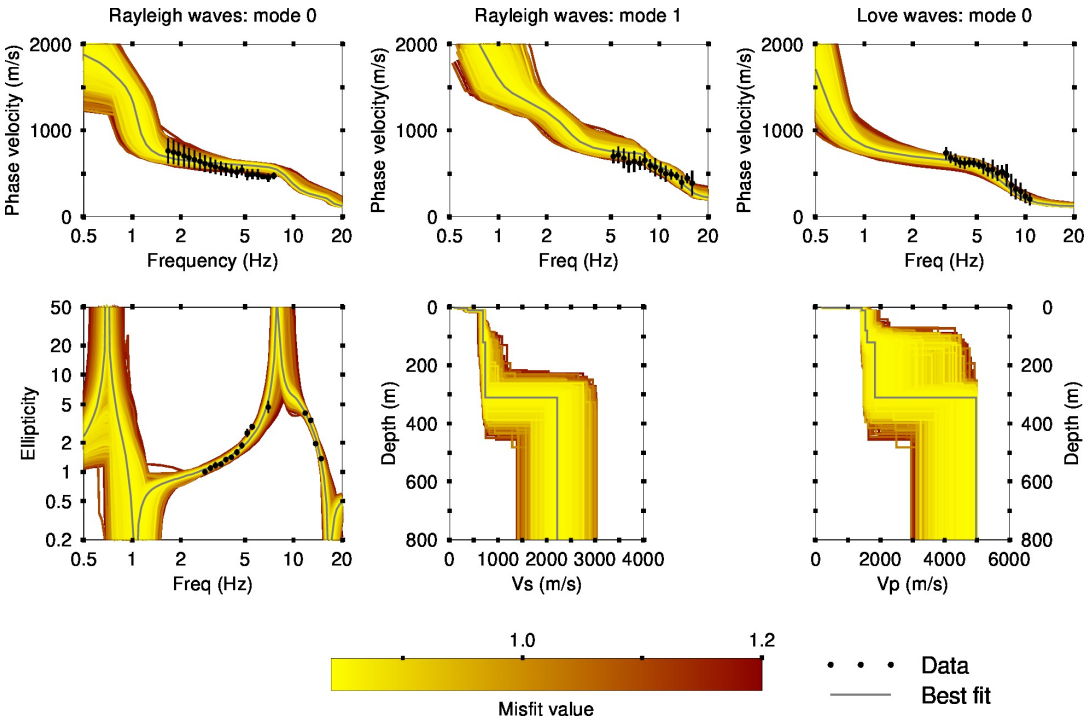

Figure 14: Inversion results using a 6LOH parametrization. The different models are shown in a color according to the misfit value, where the best model is shown in continuous grey color and the black dots indicate the data points that contribute to the inversion. The peak frequency at 0.7 Hz is used to constrain the bottom depth.

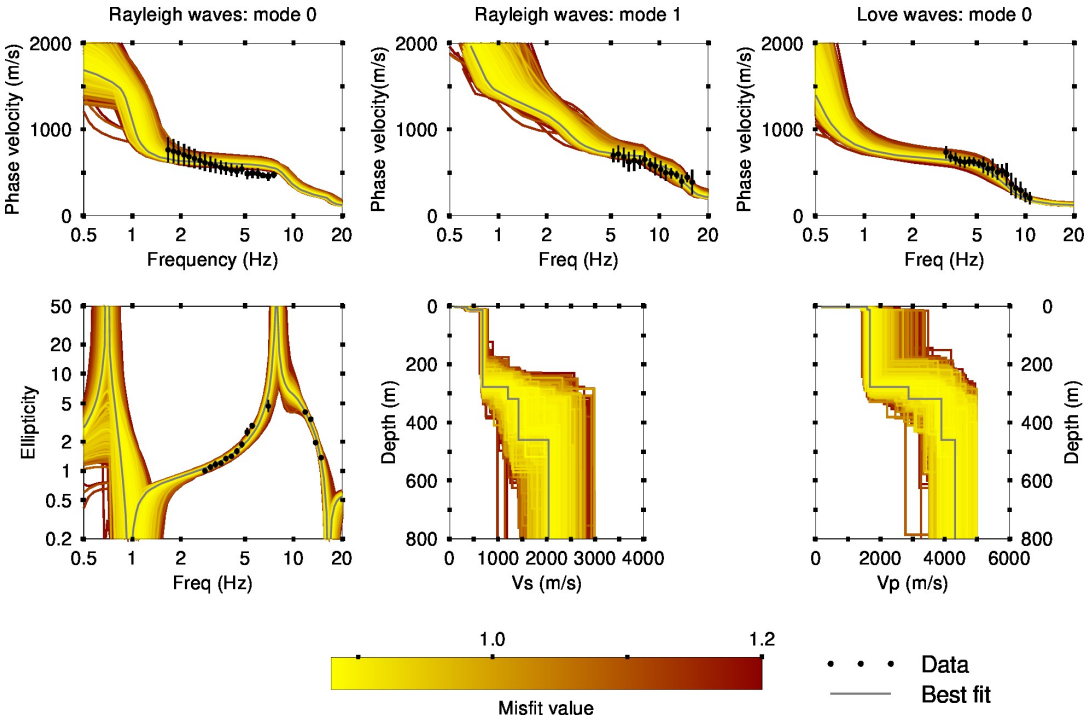

Figure 15: Inversion results using a 7LOH parametrization. The different models are shown in a color according to the misfit value, where the best model is shown in continuous grey color and the black dots indicate the data points that contribute to the inversion. The peak frequency at 0.7 Hz is used to constrain the bottom depth.

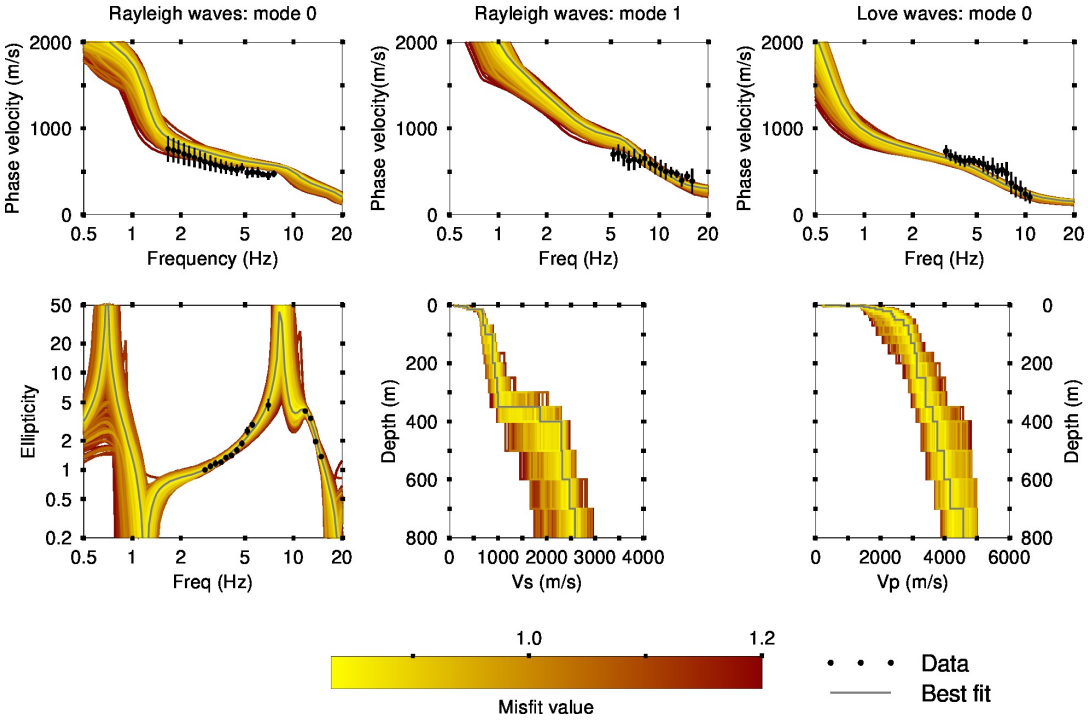

Figure 16: Inversion results using a fixed layer thickness parametrization. The different models are shown in a color according to the misfit value, where the best model is shown in continuous grey color and the black dots indicate the data points that contribute to the inversion. The peak frequency at 0.7 Hz is used to constrain the bottom depth.

6.3 Inversion summary

The best models from the inversions using different parametrizations (3LOH, 4LOH, 5LOH, 6LOH, 7LOH, and fixedLayer) are shown in Figure 17. Table 1 gives a summary of the minimum misfit values achieved in each case during the inversion process.

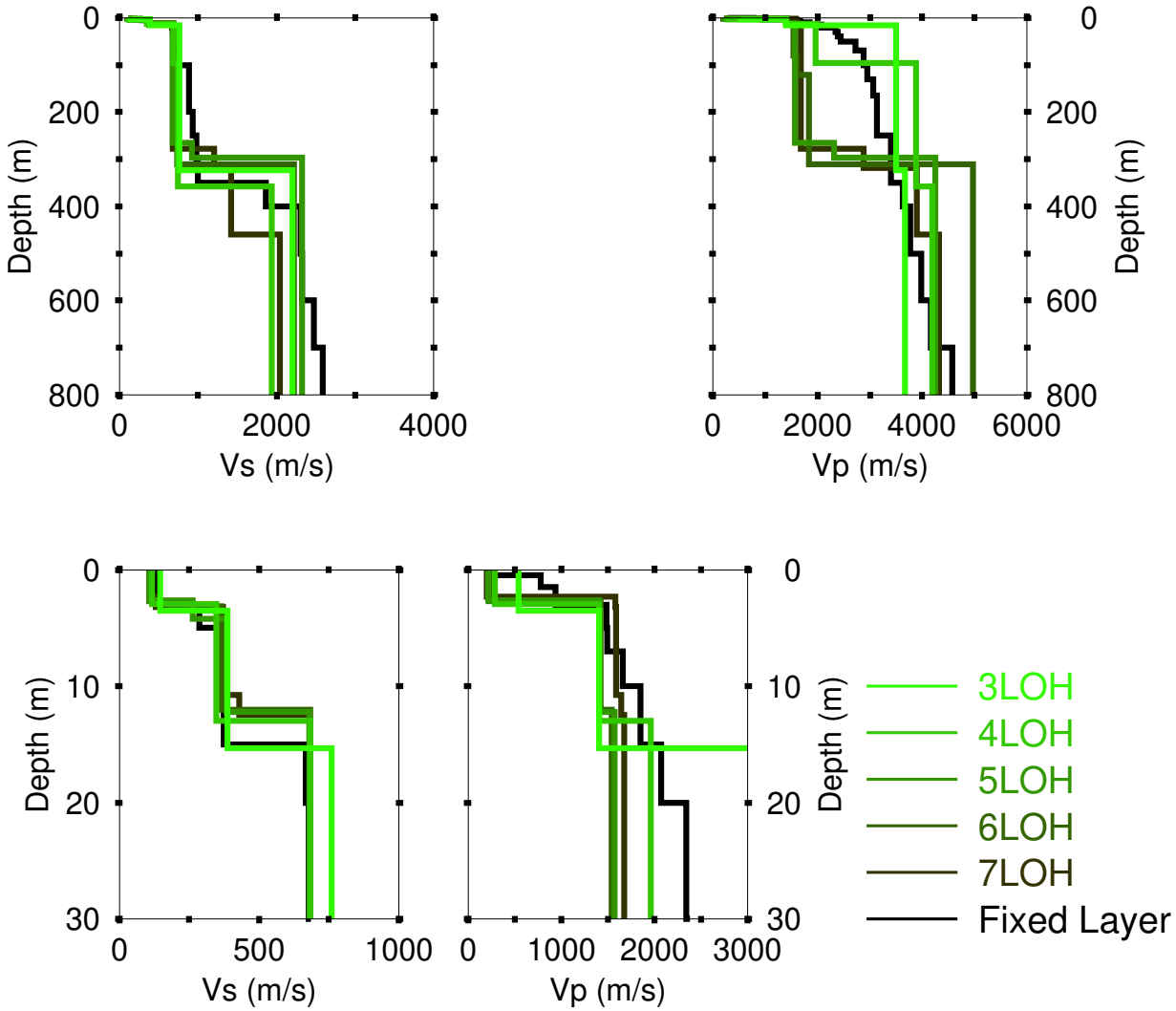

Figure 17: Overview of the best models for the different parameterizations. Top: S-wave (left) and P-wave (right) velocity profiles. Bottom: Zoom on the superficial 30 meters.

Table 1: Minimum misfit values for different parametrization.

	Minimum misfit
3 LOH	0.895935
4 LOH	0.836229
5 LOH	0.850758
6 LOH	0.844584
7 LOH	0.882737
Fixed layer	0.838064

The misfit values from the combined inversion vary in a narrow range between 0.83 and 0.9. For the different parametrizations, three major discontinuities at about 3.5, 12 and 300

m are observed. We consider all best models from the inversions are representative of the subsurface under the SSTS strong motion station. The average V_{S30} from all best models is 385.25 $\pm$ 9.43 m/s and corresponds to ground type B in EC8 (European standard) and to ground type C in SIA261 (Swiss standard).

7 Site amplification

Starting from the best models presented in Figure 17, the theoretical site amplification function is computed and compared with the empirical site amplification function of the station SSTS. The site amplification function is estimated following **?**. The comparison is shown in Figure 18.

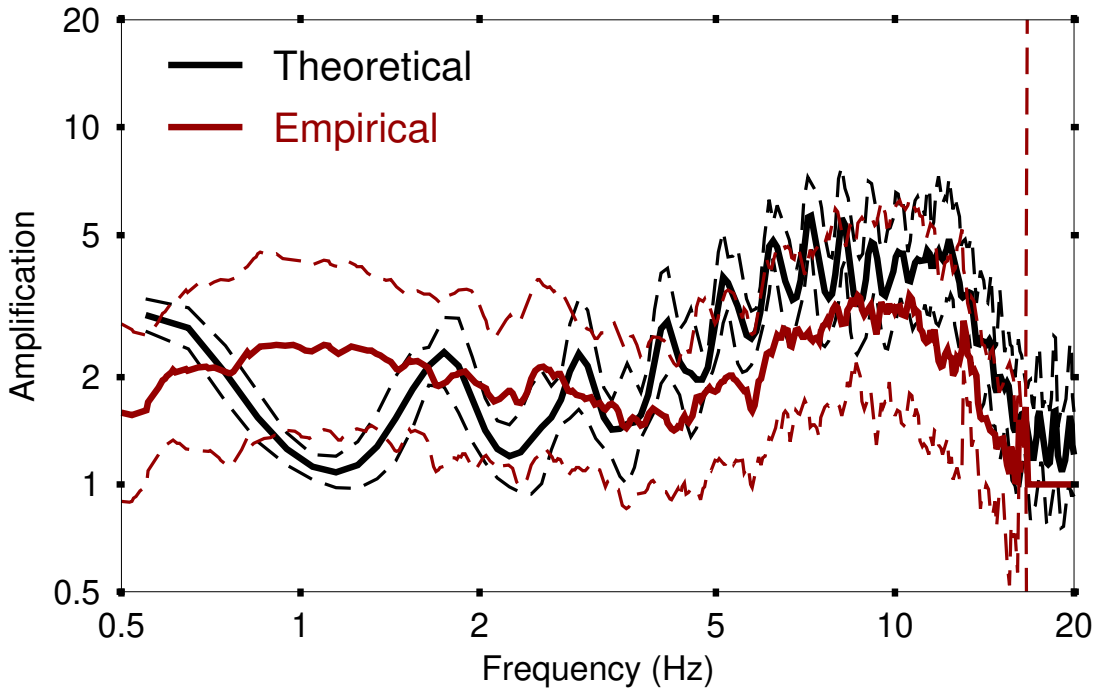

Figure 18: Comparison between the site amplification estimated for the best models from the inversions and the empirical amplification for station SSTS.

The comparison indicates that the velocity profiles from the inversion are representative of the subsurface structure under station SSTS. The empirical modeling finds a broad peak of amplification at around 1 Hz. Our inversion, however, finds a fundamental peak at around 0.7 Hz (as in the H/V measurements), followed by several peaks at higher frequencies. The overall shapes of the empirical and theoretical amplification functions are similar, but the empirical amplification is lower for frequencies above 3 Hz. This might be linked with the fact that the 1D assumption of the site is not met and site-specific amplification and deamplification effects in a complex environment lead to a different behavior.

8 Quarter-wavelength representation

The quarter wavelength representation is presented in Figure 19. The resolution is estimated down to aproximately 250 m using the ellipticity peak information.

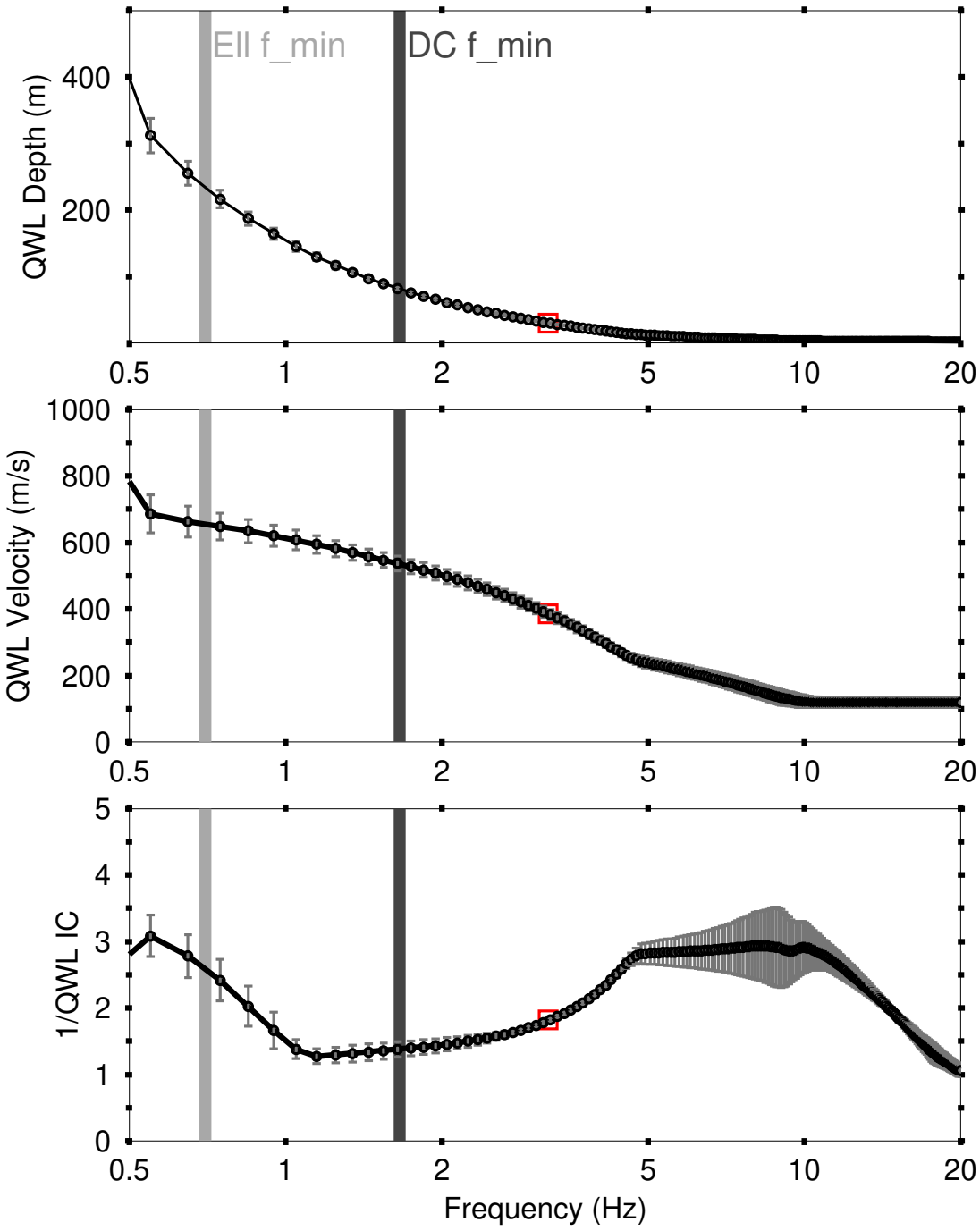

Figure 19: Quarter-wavelength representation for the best models of the inversions. The light and dark grey vertical bars indicate the minimum frequencies for the ellipticity and surface wave phase velocities, respectively, used in the inversion process.

9 Conclusion

A passive seismic survey was carried out at the strong motion station SSTS at Stans (NW) to characterize the local subsurface. The dispersion curves for Love and Rayleigh waves were estimated over a wide frequency band ranging from about 1.66 Hz to 15.95 Hz. Two frequency peaks were measured for the ellipticity in the frequency range between 0.2 and 20 Hz. The array methods used were complementary in determining different branches of the dispersion curve. It remains unclear if WaveDec and HRFK actually see different modes. The inversion allows us to resolve the shear wave velocity profile down to about 300 m.
The average V_{S30} from all best models is 385.25 $\pm$ 9.43 m/s and corresponds to ground type B in EC8 (European standard) and to ground type C in SIA261 (Swiss standard).

10 Acknowledgments

The authors thank Simon Rouwendaal for the help during the array measurements.

References

Aki, K., 1957. Space and time spectra of stationary stochastic waves, with special reference to microtremors., *Bull. Earthq. Res. Inst.*, **35**, 415–456.

Bettig, B., Bard, P. Y., Scherbaum, F., Riepl, J., Cotton, F., Cornou, C., & Hatzfeld, D., 2001. Analysis of dense array noise measurements using the modified spatial auto-correlation, *Boll. Geof. Teor. Appl.*, **42**, 281–304.

Fäh, D., Kind, F., & Giardini, D., 2001. A theoretical investigation of average H/V ratios, *Geophysical Journal International*, **145**(2), 535–549.

Hobiger, M., Bard, P.-Y., Cornou, C., & Le Bihan, N., 2009. Single station determination of Rayleigh wave ellipticity by using the random decrement technique (RayDec), *Geophysical Research Letters*, **36**(14), n/a–n/a, L14303.

Maranò, S., Reller, C., Loeliger, H.-A., & Fäh, D., 2012. Seismic waves estimation and wavefield decomposition: application to ambient vibrations, *Geophysical Journal International*, **191**(1), 175–188.

Poggi, V. & Fäh, D., 2010. Estimating rayleigh wave particle motion from three-component array analysis of ambient vibrations, *Geophysical Journal International*, **180**(1), 251–267.

Sambridge, M., 1999. Geophysical inversion with a neighbourhood algorithm—i. searching a parameter space, *Geophysical Journal International*, **138**(2), 479–494.

Wathelet, M., 2008. An improved neighborhood algorithm: Parameter conditions and dynamic scaling, *Geophysical Research Letters*, **35**(9).